Orbital anisotropy and low-energy excitations of the quasi-one-dimensional conductor β-Sr_{0.17}V_{2}O_{5}

J. Laverock, A. R. H. Preston, B. Chen, J. McNulty, K. E. Smith, L. F. J. Piper, P.-A. Glans, J.-H. Guo, C. Marin, E. Janod, and V. Ta Phuoc

Phys. Rev. B **84**, 155103 — Published 7 October 2011

DOI: 10.1103/PhysRevB.84.155103

Orbital anisotropy and low-energy excitations of the quasi-one dimensional conductor β-$Sr_{0.17}V_2O_5$

J. Laverock, A.R.H. Preston, B. Chen, J. McNulty, and K.E. Smith
Department of Physics, Boston University, 590 Commonwealth Avenue, Boston, Massachusetts, MA 02215

L.F.J. Piper
Physics, Applied Physics and Astronomy, Binghamton University, State University of New York, PO Box 6000, Binghamton, NY 13902

P.-A. Glans and J.-H. Guo
Advanced Light Source, Lawrence Berkeley National Laboratory, Berkeley, California,

C. Marin
CEA Grenoble-DSM/INAC/SPSMS, 38054 Grenoble, France

E. Janod
Institut des Matériaux Jean Rouxel-UMR 6502, Université de Nantes, 4432 Nantes, France

V. Ta Phuoc
LEMA-UMR 6157 CNRS-CEA, UFR Sciences et Techniques, Université F. Rabelais, 37200 Tours, France

Abstract

The electronic structure of the quasi-one dimensional vanadium beta-bronze β-$Sr_{0.17}V_2O_5$ has been measured in detail using soft x-ray absorption spectroscopy, x-ray emission spectroscopy, and resonant inelastic soft x-ray scattering. Together, these measurements have been used to derive the experimental site-resolved (*k*-integrated) band structure of a material whose electronic structure is difficult to obtain from first principles. The occupied states, probed by x-ray emission measurements, demonstrate the O 2*p* - V 3*d* bonding hybridization at the bottom of the O 2*p* band, with the V $3d_{xy}$ 'magnetic orbitals' well-separated in energy. These results are consistent with the carriers being small polarons. The strong anisotropy in the absorption spectrum is used to identify the energy and character of the unoccupied states. Additionally, absorption measurements at the V *L*-edge are compared with atomic multiplet calculations, clarifying the interpretation of the experimental multiplet structure and consistent with the presence of both V^{5+} and V^{4+} species. Site specific electronic excitations, probed by resonant inelastic x-ray scattering at the V *L*-edge, are observed

at an energy of 1.1 eV, and are suggested to correspond to transitions from the partially-filled d_{xy} magnetic orbital into the unoccupied $d_{xy,yz}$ orbitals.

Introduction

Transition metal oxide bronzes exhibit a wide range of fascinating ordering phenomena, including metal-insulator transitions (MIT), superconductivity, spin-ladder and spin-Peierls behavior.[1-4] In particular, the quasi-one dimensional vanadium beta-bronzes (β-$A_xV_2O_5$) have garnered substantial interest recently owing to the observation of an MIT for x = 0.33 and superconductivity under pressure (for β-$Na_{0.33}V_2O_5$ and β-$Cu_{0.65}V_2O_5$).[3-5] These highly anisotropic ($\rho_c/\rho_b \approx 100$) compounds,[3] which can be prepared with either monovalent ($A = Li^+$, Na^+, Ag^+) or divalent ($A = Ca^{2+}$, Sr^{2+}) cations, have a mixed valence of V^{4+} (d^1) and V^{5+} (d^0), and the V 3*d* electrons are thought to predominantly reside on just one of the three inequivalent V sites.[6] For the stoichiometric compounds (x = 1/3), a charge-ordered phase develops below 230 K, followed by an MIT at ~ 130 K. However, the nature of the MIT is still under debate. Several studies agree that the charge carriers are most likely small polarons,[1,7-9] but angle-resolved photoemission measurements are consistent with both weak coupling (charge-density waves) and strong coupling (polarons) features.[7] Indeed, the low dimensionality raises important questions regarding the interplay between electron-electron interactions (e.g. Luttinger liquid behavior)[10] and electron-phonon coupling (e.g. charge-density wave or polaronic behavior).[9] Despite the rich electronic and structural phase diagrams of the vanadium beta-bronzes, there have been relatively few experimental investigations into the electronic structure of these materials, and *ab initio* calculations are hampered by the large unit cell (particularly if the disordered occupation of the cations is properly included).

We report here a study of the electronic structure of β-$Sr_{0.17}V_2O_5$ using synchrotron radiation-based soft x-ray emission and absorption spectroscopies. The crystal structure of β-$Sr_{0.17}V_2O_5$ consists of sheets of strongly distorted VO_6 octahedra stacked in the *b*-axis.[11] The octahedra form pairs in the *a*-*c* plane, leading to pairs of chains (i.e. two leg ladders) along the *b* crystallographic direction, as illustrated in Fig. 1. For β-$Sr_{\approx 1}V_2O_5$, a doubling of the unit cell along the *b*-axis is induced by the zig-zag ordering of the Sr^{2+} cations. The three inequivalent V ions in the structure form three distinct polyhedra: $V1O_6$, $V2O_6$ and $V3O_5$. These combine to form two almost orthogonal ladder structures; V1-O-V3 rungs are aligned close to the *c*-axis and V2-O-V2 rungs are oriented close to the *a*+*c* direction. The nature of the distortions to the octahedra reflect the tendency of the V ion to form a (multiple) vanadium-oxygen covalent

(vanadyl) bond with the apical oxygen (O_{ap}), contracting the V-O_{ap} bond distance. (The corresponding extension of the distance to the sixth oxygen, particularly for V3, leads to the common consideration of the polyhedra as distorted square pyramids). This apical bond is important in that it provides a local quantification axis for the vanadium atom.[12] In Fig. 1, we consider the *z* axis as collinear to the V-O_{ap} bond, and the *x* and *y* axes point (almost) to the basal plane oxygens. The distorted octahedral crystal field approximately splits the V 3*d* states into t_{2g} (d_{xy}, d_{xz}, and d_{yz}), and e_g states ($d_{x^2-y^2}$ and d_{z^2}). Based on qualitative molecular orbital arguments,[1] the V-O_{ap} bond forms three bonding/antibonding orbitals: one σ-bonded d_{z^2} orbital and two (almost degenerate) π-bonded orbitals (d_{xz}, and d_{yz}).[12] Of the e_g states, the σ-bonded d_{z^2} state is the most unstable and lies highest in energy. Conversely, the d_{xy} orbital is the most stable of the t_{2g} states. The Sr^{2+} ion donates 0.17 electrons per V atom and these electrons are expected to occupy the V d_{xy} magnetic orbitals. In fact, electron spin resonance measurements of isoelectronic β-$Na_{0.33}V_2O_5$ (whose room-temperature phase is found to be qualitatively very similar to β-$Sr_{0.17}V_2O_5$)[9] have demonstrated the preferential occupation of the V1 sites,[6] which has also been suggested by optical measurements,[13] and is in agreement with expectations from bonding considerations.[1]

Experimental

Crystals of β-$Sr_{0.17}V_2O_5$ were grown by the traveling solvent floating zone technique.[9,14] Neutron diffraction measurements suggest the sample is composed of several large grains with dimensions of a few mm. The grains are highly oriented along the *b*-axis, with a slight misorientation (< 3°) along *c*. Note that the grains are larger than the size of the x-ray beam spot (and the misorientation is smaller than the angular resolution of the measurements), and our x-ray measurements are therefore not sensitive to the grain structure. These crystals were cleaved in air to expose the *b*-*c* plane. Measurements were carried out using the AXIS endstation of beamline 7.0.1 at the Advanced Light Source, Lawrence Berkeley National Laboratory. X-ray absorption measurements were made in both total electron yield (TEY) and total fluorescent yield (TFY) modes with a beamline energy resolution of 0.2 eV full width at half maximum (FWHM). The photon energy was calibrated using reference spectra recorded at the Ti *L*-edge and O *K*-edge from TiO_2. X-ray emission spectra were recorded with a Nordgren-type grating spectrometer set to an energy resolution of 0.5 eV FWHM. For resonant spectra recorded at the V L_3 and O *K*-

edges, the beamline resolution was set to 0.5 eV. Emission spectra were calibrated using a Zn metal reference spectrum. Polarization-dependent measurements were made with the polarization vector of the normally incident x-rays aligned (to within ~ 3°) with both the *b*-axis grains ($E \parallel b$) and perpendicular to them ($E \parallel c$), as well as at near-grazing incidence (i.e. $E \parallel a$ to within ~ 10°).

The organization of the manuscript is as follows. First, XAS measurements at the V $L_{3,2}$-edge are presented and discussed through comparison with atomic multiplet calculations. These measurements are sensitive to the local atomic environment of the V site, and are a sensitive probe of the crystal field and oxidation state. Secondly, the electronic band structure is investigated via O *K*-edge XAS (unoccupied states) and XES (occupied states). Resonant measurements at the V L_3-edge are shown, providing additional information on the occupied V 3d states. Finally, the technique of RIXS is applied to reveal local electronic excitations. Together, these complementary techniques provide a complete picture of the site-resolved density of states of β-$Sr_{0.17}V_2O_5$, a material that is of particular interest owing to its one-dimensional electronic behavior, but whose electronic structure is difficult to obtain from first principles.

X-ray absorption spectroscopy

Figure 2a presents V $L_{3,2}$ -edge XAS spectra from β-$Sr_{0.17}V_2O_5$ measured in both TEY and TFY modes for different incident light polarizations. The similarity between the TEY spectra (with a probing depth of ~ 10 nm) and the TFY spectra (with a probing depth of ~ 100 nm) demonstrate that we are measuring the bulk electronic structure of the sample. The two main peaks in the spectra at ~ 518 eV and ~ 525 eV correspond to V L_3 and L_2 absorption, respectively; i.e. transitions from the spin-orbit split V $2p_{3/2}$ and V $2p_{1/2}$ core levels to unoccupied V 3*d* orbitals. Unlike *K*-edge spectra, which can provide a direct measure of the unoccupied partial density-of-states (PDOS), transition metal *L*-edge spectra are dominated by interactions between the 2*p* core hole and the valence wavefunctions (multiplet effects), and are strongly sensitive to the site symmetry and oxidation state of the transition metal, as well as its crystal field splitting.[15] In vanadium dioxide, VO_2, Haverkort *et al.* recently used their V *L*-edge spectra, including their polarization anisotropy, to probe the changes in the V 3*d* orbital occupation across the MIT.[16] However, as shown in Fig. 2a, we find only very weak dependence of the *L*-edge XAS spectra from β-$Sr_{0.17}V_2O_5$ on the incident photon polarization. There is a shift to higher absorption energy of approximately 0.2 eV, and a small change in the branching ratio between L_3

and L_2 transitions for $E \parallel b$ compared with $E \parallel a,c$. A similar weak anisotropy at this edge has been reported for α′-NaV_2O_5.[17]

The spectra presented in Fig. 2a are reminiscent of other d^0 vanadium oxides, e.g. V_2O_5 and HfV_2O_7,[18] which is consistent with the charge state of β-$Sr_{0.17}V_2O_5$ being close to +5. Moreover, the spectra are in good qualitative agreement with XAS measurements of the isoelectronic β-$Na_{0.33}V_2O_5$ (in polycrystalline form),[19] where the observation of a pronounced knee ~ 1.5 eV below the L_3 peak was interpreted as arising from the crystal field splitting, and its suppression compared with the splitting at the O *K*-edge (~ 2.1 eV) was taken as evidence for the mixed valence (V^{4+} and V^{5+}) of vanadium. In our data, we observe a similar knee, located at -1.4 eV from the L_3 peak and indicated by the arrow in Fig. 2a, alongside an additional feature at -2.4 eV. Both of these features are clearly identifiable in the first derivative of the data. Atomic multiplet calculations of V^{5+} in either octahedral or tetragonal symmetry (see Fig. 3) fail to reproduce the -1.4 eV feature for any reasonable parameters of the crystal field, but the -2.4 eV peak is captured well with $10Dq$ = 2.1 eV – 2.4 eV (representing the splitting between the t_{2g} and e_g states in the crystal field, see Fig. 2b). On the other hand, the -1.4 eV peak can be attributed to the presence of occupied V^{4+} species (the formal valence of β-$Sr_{0.17}V_2O_5$ being +4.83); as shown in Fig. 2b, the V^{4+} peak (in the same crystal field) has its principle L_3 peak -1.4 eV from the V^{5+} peak. However, the atomic multiplet calculations, whilst capturing the principal features of the experimental spectra, do not reproduce the measured width, as exemplified in the linear superposition of the V^{4+} and V^{5+} spectra shown in Fig. 2b. As demonstrated by Fig. 3c, the shape of the spectra strongly supports a tetragonal distortion to the crystal field. The satellite structures at -2.4 eV from the L_3-edge and -1.8 eV from the L_2-edge are found to be too intense for O_h symmetry. However, the tetragonal (D_{4h}) distortion (in the form of the D_s and D_t parameters) accompanies a suppression and shift in energy of the satellites for reasonable values of D_s and D_t ~ 0.05 – 0.15 eV.

XAS at the O *K*-edge corresponds to transitions from the O 1*s* core level to unoccupied O 2*p* states, and these transitions are easily interpreted in terms of the delocalized electron states; the spectrum closely resembles (with the exception of the effects of the core-hole) the unoccupied O 2*p* PDOS. In Fig. 4, the O *K*-edge spectra from room temperature β-$Sr_{0.17}V_2O_5$ are presented for several different polarizations of the incident light. As for the V *L*-edge data, the TEY and TFY data are found to be similar, reinforcing the idea that our measurements are representative of

the bulk electronic structure. This is also supported by the similarity of the spectra for polarizations parallel to the *a*- and *c*-axes, which were recorded at near-grazing (which is more surface sensitive) and normal incidence respectively. No significant temperature dependence was observed in either the V *L*- or O *K*-edge spectra between samples held at room temperature and at 88 K. Owing to the geometry of the VO_6 polyhedra, the x-rays couple to O p_y orbitals for $E \parallel b$, and to a combination of O p_x and p_z orbitals for $E \parallel a$ or c (see Fig. 1). The spectra recorded with the Poynting vector parallel to the *a*- and *c*-axes of the crystal are qualitatively similar, exhibiting strong features at 529.5 eV (point A in Fig. 4) and 531.2 eV (point C) that can be attributed to hybridization of the O 2*p* states with the V t_{2g} and e_g states. An additional shoulder on the high energy side of peak C is evident in both these spectra at 531.9 eV (point D), and may represent the high-energy side of the e_g manifold. These lead to a measured crystal-field splitting of $\sim 1.7 - 2.4$ eV, in good agreement with suggestions from band structure calculations of the isostructural and isoelectronic β-$Na_{0.33}V_2O_5$,[19] as well as being consistent with our V *L*-edge XAS data. It is emphasized that, owing to the distorted $V1O_6$, $V2O_6$ and $V3O_5$ polyhedra, these are not degenerate V t_{2g} and e_g states, but the terms are used here to refer to the two principle peaks in the V PDOS. At higher energies (not shown, 537 – 545 eV), a weak, broad peak emerges due to hybridization with the V 4*sp* states.

In contrast to the spectra for the *a*- and *c*-axes discussed above, the spectrum for $E \parallel b$ shows pronounced anisotropy, which might be expected for such a crystallographically anisotropic material. Peaks C and D (representing the higher e_g states) in Fig. 4 are strongly suppressed, and the intensity maximum in the low-energy t_{2g} manifold is shifted upwards by 0.2 eV to 529.7 eV (point B). This anisotropy can be understood by comparison with V_2O_5: the basic building blocks of strongly distorted VO_6 octahedra (or VO_5 square pyramids) are similar (although their arrangement in the crystal structure is quite different). In V_2O_5, the vanadyl bonds are aligned along the *c*-axis,[20] and polarization-dependent XAS measurements of the O *K*-edge reveal a substantial growth in the intensity of the e_g peak as the polarization vector is rotated from perpendicular to collinear to the vanadyl bond.[21] Such angular dependence of the XAS spectra can be understood from *ab initio* band structure calculations of V_2O_5,[22] which suggest that the dominant hybridization of the e_g states is with the O_{ap} p_z orbitals of the vanadyl bond. For β-$Sr_{0.17}V_2O_5$, the vanadyl bonds of the V1, V2 and V3 polyhedra are approximately aligned in the crystallographic *a*+*c*, *c* and *a* directions respectively (i.e. they are all in the *a*-*c* plane, see

Fig. 1), leaving the *b*-axis as the unique dimension that does *not* pick up a contribution from these e_g states.

The presence of a second e_g peak in XAS spectra has also been observed for V_2O_5, located ~ 1.2 eV above the main peak, and becoming most strong for $E \parallel z$,[21] as well as separated by ~ 1 eV for α′-NaV_2O_5.[17,23] This splitting of the e_g manifold is consistent with estimates of the separation between the bottom (owing to $d_{x^2-y^2}$ orbitals) and top (owing to d_{z^2} orbitals) of the manifold from band calculations of both V_2O_5 (~ 1.2 eV)[22] and α′-NaV_2O_5 (~ 0.8 eV).[24] In our data, we find two features separated by ~ 0.7 eV associated with the e_g manifold (peaks C and D), which can be ascribed to the bottom (i.e. $d_{x^2-y^2}$) and top (i.e. d_{z^2}) of the e_g density of states.

We also note that the increase in the intensity of the e_g peak in the V_2O_5 data of Ref.[21] was accompanied by a decrease in the intensity of the t_{2g} peak, and that for polarizations midway between the basal plane and the vanadyl bond direction the intensity of the two peaks was found to be approximately equal. The multiple orientations of the vanadyl bond in β-$Sr_{0.17}V_2O_5$ mean that for polarizations anywhere in the *a*-*c* plane, we are sensitive to an average of the local *x* and *z* axes, and the slightly different ratio between the t_{2g} (peaks A and B) and e_g (peaks C and D) features for $E \parallel a$ and $E \parallel c$ presumably reflects differences in the precise angle in the *a*-*c* plane of the measurement.

The shift in the t_{2g} peak (by ~ 0.2 eV) observed in Fig. 4 between peaks A and B (for $E \parallel a,c$ and $E \parallel b$ respectively) may reflect the slightly different sensitivities of the two polarizations to the unoccupied d_{xy} orbitals and $d_{xz,yz}$ orbitals. Band structure calculations show a clear separation in energy between these two orbitals for both V_2O_5 and α′-NaV_2O_5, while for V_2O_5 the hybridization of the two orbitals is clearly split between O3 p_y orbitals and O2 $p_{x,y}$ orbitals (of a different O site) respectively.[22,24] A similar (albeit larger) shift in the onset of the O *K*-edge XAS was observed for α′-NaV_2O_5 and was interpreted as excitation into different O sites.[23]

X-ray Emission Spectroscopy

X-ray emission spectroscopy (XES) measures the occupied valence band PDOS in solids.[25-26] XES spectra taken well above the O *K*-edge absorption threshold (at 550 eV) are shown in Fig. 5 for different polarization vectors of the incident x-rays; also shown are the O *K*-edge XAS spectra from Fig. 4. The final state of the XAS process involves a core hole that shifts the spectra to lower energies; in Fig. 5 the O *K*-edge spectra have been shifted by +1 eV to

(approximately) account for the effect of the core hole (core-hole shifts of 1 eV have previously been observed for transition metal oxides).[27] The anisotropy observed in the XAS spectra is not so strongly present in the XES spectra of Fig. 5, with only a small difference in the shape of the profiles, particularly near the peak of the spectra (at ~ 526 eV). This weaker anisotropy in the occupied states is expected since the O 2*p* states are (nominally) fully occupied. The O 2*p* states span the energy range roughly -7 eV to -2 eV (522 eV to 527 eV) below the onset of the XAS spectra, in excellent agreement with the predictions of the local density approximation,[19] with the majority of the weight near the upper end of this range. Towards the bottom of the O 2*p* band, a shoulder is evident between 522 eV and 524 eV, and is associated with the π and σ covalent bonding hybridization with the V 3*d* states.

Band calculations of the electronic structure of β-$A_xV_2O_5$ predict a metallic ground state, with dispersive bands crossing E_F along the *b*-axis, in agreement with the anisotropy observed in resistivity measurements, ($\rho_c/\rho_b \approx 100$).[3] However, whilst the occupied V d_{xy} orbitals are not expected to hybridize strongly with the O 2*p* states (and are therefore expected to be very weak in the O 2*p* XES spectrum), the lack of a Fermi edge in the XES spectra is in agreement with angle-resolved photoemission spectra of the isoelectronic β-$Na_{0.33}V_2O_5$.[7] The absence of spectral weight near E_F in photoemission measurements has been interpreted as evidence for the charge carriers being small polarons,[7] as suggested by Goodenough,[1] and demonstrated via optical measurements.[8-9]

By tuning the incident photon energy to a feature of the absorption spectrum, we can resonantly excite the system according to that particular transition, thereby measuring the occupied PDOS associated with that particular state. Shown in Fig. 5 are resonant XES (RXES) spectra excited at the first peak of the XAS spectra (points A and B in Fig. 4, corresponding to the t_{2g} states) for incident polarization parallel to the *b* and *c* crystallographic axes. (The weak peak at ~ 529.5 eV is due to elastically scattered incident photons.) These spectra are narrower than the above-threshold XES spectra shown in Fig. 5, and are centered about 1 eV lower in energy. Most notably, the shoulder that was previously associated with V hybridization, located towards the bottom of the XES spectra, is more pronounced for $E \parallel c$ than for $E \parallel b$. Since these states are associated with the V 3*d* - O 2*p* bonding orbitals, this indicates that the p_y orbitals are less involved in the covalent bonding.

For α'-NaV_2O_5, resonant excitation at the onset of the t_{2g} states was found to correspond to states towards the bottom of the O 2*p* band,[23,28] in agreement with our findings. In those measurements, the above-threshold data also had a substantially stronger low-energy shoulder, presumably indicating the greater number of V 3*d* electrons available to participate in bonding.

Resonant Inelastic X-ray Spectroscopy

By resonantly exciting electrons near the transition metal *L*-edge, it is possible to probe both local and coherent excitations of the system in a process known as resonant inelastic x-ray spectroscopy (RIXS). For the V d^1 system, the excitation process is $2p^6 3d^1 \rightarrow 2p^5 3d^2 \rightarrow 2p^6 3d^{1*}$, in which the first process involves a transition similar to the XAS absorption process, leaving the system with a 2*p* core-hole, which decays via the second process. The final state may be in an excited state, denoted by *, in which the excitation can be local crystal-field excitations (dipole forbidden *d*-*d** transitions), O 2*p* – V 3*d* charge-transfer excitations, or even collective excitations such as magnons. The separation of PDOS features (of constant emission energy) from RIXS features (of constant loss energy) can be achieved by inspecting their dependence on the incident photon energy.[26,29]

Fig. 6a shows the V L_3-edge RIXS spectra for several different incident photon energies with the incident polarization parallel to the crystallographic *a*-axis. Three main features are observed in these spectra. Firstly, a broad peak between 505 eV and 513 eV is present in the emission spectra (peak B), and since it is constant in emission energy can be associated with the V PDOS of hybridized V 3*d* - O 2*p* bands. A second feature that is also constant in emission energy (peak A) is visible at lower intensity between 514 and 516 eV, and can be attributed to the occupied V 3*d* PDOS. For α'-NaV_2O_5, Schmitt *et al.* found V PDOS features centered at ~ 510 eV (corresponding to the O 2*p* hybridized states) and at ~ 515 eV (corresponding to the occupied V 3*d* states), which agrees very well with our peaks. Thirdly, for the lowest incident photon energy, E_{in} = 515.2 eV, a shoulder to the low-energy side of peak B emerges. A similar scenario was observed for α'-NaV_2O_5,[28] and was interpreted as charge-transfer excitations superimposed upon the PDOS features. Such an explanation seems to be appropriate here too, putting the energy of the O 2*p* – V 3*d* charge transfer excitation at ~ 6 eV.

Finally, for the E_{in} = 515.2 eV spectrum, a strong peak at ~ 514 eV, not immediately visible in the other spectra, is evident. Plotting these spectra on an energy-loss scale, shown in Fig. 6b,

reveals that this peak has a center at ~ 1.1 eV. In α'-NaV_2O_5, *dd** excitations were observed in RIXS spectra at ~ 1.5 eV, and were attributed to Hubbard excitations into the upper Hubbard band.[30] However, this assignment proved controversial, and these peaks have been re-interpreted as deriving from *dd** excitations from occupied d_{xy} orbitals to unoccupied $d_{xz,yz}$ orbitals.[31-32] It is also worth noting that weight at this energy transfer also exists for higher excitation energies, but is obscured by the presence of the fluorescent PDOS features. In Fig. 6b, the dotted lines show the spectra with the elastic peaks (of fixed width corresponding to the experimental resolution) and fluorescent features removed. The shape of the fluorescent contribution to the E_{in} = 518.7 eV spectrum, in which it is well separated from other spectral features, was approximated by a Gaussian and subtracted from the other spectra. Although the subtracted spectra are noisy, owing to the crude approximation to the fluorescent contribution (and its incomplete subtraction), appreciable intensity is evident for all spectra at -1.1 eV energy transfer, indicating that the *dd** feature is also present at other incident photon energies. Additionally, the transitions within the V1-O-V3 ladder (at 0.85 – 1 eV) that have been observed in optical measurements,[9,13] are not permitted in the RIXS process, since they are not local charge neutral excitations.[31] In Fig. 6c, the energy loss spectra are shown for $E \parallel b$, and exhibit similar features (including the ~ 1.1 eV peak), although at a much weaker intensity (which may be associated with the geometry of the measurements).

Conclusions

We have presented a detailed soft X-ray spectroscopic study of the electronic structure of the quasi-one dimensional vanadium beta-bronze β-$Sr_{0.17}V_2O_5$. X-ray emission measurements show that the valence band, predominantly of O 2*p* character, exhibits appreciable hybridization with the V 3*d* states towards its lower range, associated with the V 3*d* bonding orbitals. Polarization-dependent x-ray absorption measurements at the O *K*-edge reveal strong hybridization of the unoccupied V 3*d* states with O 2*p* character and pronounced anisotropy of these states. V t_{2g} states are separated from e_g states by ~ 1.7 – 2.4 eV, providing a direct experimental measure of the crystal field splitting, which is in good agreement with expectations from band structure calculations. A small shift (~ 0.2 eV) in the energy of the t_{2g} peak with different incident light polarizations suggest that the t_{2g} DOS is relatively narrow and the lifting of the degeneracies of the constituent orbitals is quite weak. On the other hand, for the e_g states,

a separation of ~ 0.7 eV is observed between the $d_{x^2-y^2}$ and d_{z^2} orbitals. Together, these results provide an experimental measurement of the *k*-integrated, site-resolved band structure of β-$Sr_{0.17}V_2O_5$, shown in Fig. 7. X-ray absorption measurements at the V *L*-edge were compared with atomic multiplet calculations, and are consistent with the presence of both V^{5+} and V^{4+} species. The ~ 1.4 eV satellite feature at this edge is found to be associated directly with the V^{4+} multiplet structure, rather than the crystal field splitting, which is rather responsible for a feature at ~ 2.4 eV from the L_3-edge peak. Site specific crystal-field excitations have been measured with resonant inelastic x-ray scattering at the V *L*-edge, in which a peak at 1.1 eV is argued to correspond to transitions from the partially-filled d_{xy} magnetic orbital into the unoccupied $d_{xz,yz}$ orbitals.

Acknowledgments

The Boston University (BU) program is supported in part by the Department of Energy under Contract No. DE-FG02-98ER45680. The Advanced Light Source is supported by the Director, Office of Science, Office of Basic Energy Sciences, of the U.S. Department of Energy under Contract No. DE-AC02-05CH11231.

Figure Captions:

Figure 1:

(Color online) The crystal structure of β-$Sr_{0.17}V_2O_5$ projected along the *b* crystallographic axis, showing the orientation of the VO5 square pyramids. At the bottom, the orientation of each of the $V1O_5$, $V2O_5$, and $V3O_5$ pyramids are shown with the vanadyl bond (V-O_{ap}) aligned with the paper vertical, representing their local quantification axes (*x*, *y* and *z*). The Sr positions are partially occupied.

Figure 2:

(Color online) (a) V $L_{3,2}$ -edge XAS spectra of β-$Sr_{0.17}V_2O_5$ recorded in TEY (solid lines) and TFY (open symbols) modes. To illustrate the isotropy at this edge, the TFY data is shown for light incident parallel to both the *a*- and *b*-axes. The first derivative of the TEY data is shown at the bottom of the figure for $E \parallel a$; the arrows indicate features associated with local minima. (b) V $L_{3,2}$-edge atomic multiplet calculations for V^{5+} and V^{4+} in a tetragonal (D_{4h}) distortion to octahedral symmetry (the parameters of the calculation are $10Dq$ = 2.1 eV, $D_t = D_s$ = 0.1 eV) using the CTM4XAS program.[33] These spectra have been shifted by -1.4 eV to align with the measured L_3-edge . The dashed (green) line in (b) shows the linear superposition of the V^{5+} and V^{4+} spectra at a ratio of 0.83:0.17 according to the stoichiometry.

Figure 3:

(Color online) V $L_{3,2}$-edge atomic multiplet calculations of V^{5+} and V^{4+} in octahedral (O_h) and tetragonal (D_{4h}) symmetry. (a) The dependence of the calculated spectra of V^{5+} on the crystal field splitting, $10Dq$, in O_h symmetry. Spectra are shown vertically offset for clarity. (b) Dependence of the V^{4+} spectra on $10Dq$. Also shown in thick red is the V^{4+} spectrum in D_{4h} symmetry for $D_t = D_s$ = 0.1 eV. (c) The dependence of V^{5+} spectra on D_s and D_t (D_{4h} symmetry). (d) The effect of reducing the magnitude of the Slater integral in O_h symmetry for V^{5+}.

Figure 4:

(Color online) Polarization dependence of O *K*-edge XAS spectra, recorded in both TEY (solid lines) and TFY (circles) modes.

Figure 5:

(Color online) Polarization-dependent above-threshold O *K*-edge XES spectra of β-$Sr_{0.17}V_2O_5$ recorded with the sample at room temperature, alongside RXES spectra recorded with a photon energy of 529.7 eV (the arrow indicates the location of elastically scattered x-rays). The solid line is a guide to the eye and represents a binomial smoothing of the raw XES data. Also shown are the O *K*-edge TEY XAS spectra from Fig. 3. For comparison, the leading edge of the TFY data is also displayed by the empty circles. Note that the XAS spectra have been offset by +1 eV with respect to Fig. 3 to account for the core-hole shift (see text).

Figure 6:

(Color online) V L_3-edge RIXS spectra for a) and b) $E \parallel a$, and c) $E \parallel b$ recorded at the incident photon energies shown on the V L_3-edge XAS spectrum in the inset to a). The data are shown on an absolute energy scale in a), and on a loss energy scale in b) and c). The regions marked A and B represent the occupied V 3*d* states and their hybridization with the O 2*p* states respectively. The gray regions in b) and c) show the elastically scattered light, and the dotted line at -1.1 eV demonstrates the *dd** excitation feature. In b) the dotted lines correspond to the data with the elastic peak and V 3*d* fluorescent contribution removed (see text), demonstrating the presence of the -1.1 eV RIXS peak at other photon energies.

Figure 7:

(Color online) Schematic energy level diagram for β-$Sr_{0.17}V_2O_5$ based on the experimental results. The locations of the occupied states are estimated from the onset of the XES and RIXS spectra. Similarly, the unoccupied states are derived from the O *K*-edge XAS spectra; the black solid lines represent the peak positions within the approximate bandwidth of the state. Also shown is the *dd** excitation revealed by RIXS measurements.

1. J.B. Goodenough, Progress in Solid State Chemistry **5**, 145 (1971).
2. Y. Ueda, Chemistry of Materials **10**, 2653 (1998); X. Xu, A.F. Bangura, J.G. Analytis, J.D. Fletcher,

M.M.J. French, N. Shannon, J. He, S. Zhang, D. Mandrus, R. Jin, and N.E. Hussey, Physical Review Letters **102** (2009).
3. H. Yamada and Y. Ueda, Journal of the Physical Society of Japan **68**, 2735 (1999).
4. T. Yamauchi, Y. Ueda, and N. Môri, Physical Review Letters **89**, 057002 (2002).
5. Y. Ueda, M. Isobe, and T. Yamauchi, Journal of Physics and Chemistry of Solids **63**, 951 (2002).
6. M. Heinrich, H.A.K. von Nidda, R.M. Eremina, A. Loidl, C. Helbig, G. Obermeier, and S. Horn, Physical Review Letters **93**, 116402 (2004).
7. K. Okazaki, A. Fujimori, T. Yamauchi, and Y. Ueda, Phys Rev B **69**, 140506 (2004).
8. C. Presura, M. Popinciuc, P.H.M. van Loosdrecht, D. van der Marel, M. Mostovoy, T. Yamauchi, and Y. Ueda, Physical Review Letters **90**, 026402 (2003).
9. V. Ta Phuoc, C. Sellier, B. Corraze, E. Janod, and C. Marin, The European Physical Journal B - Condensed Matter and Complex Systems **69**, 181 (2009).
10. T. Giamarchi, Phys Rev B **44**, 2905 (1991).
11. A.D. Wadsley, Acta Crystallographica **8**, 695 (1955).
12. M.L. Doublet and M.B. Lepetit, Physical Review B (Condensed Matter and Materials Physics) **71**, 75119 (2005).
13. V. Ta Phuoc, C. Sellier, and E. Janod, Physical Review B (Condensed Matter and Materials Physics) **72**, 35120 (2005).
14. V. Ta Phuoc, C. Sellier, E. Janod, and C. Marin, Physical Review B (Condensed Matter and Materials Physics) **77**, 075123 (2008).
15. F.M.F. de Groot, Coordination Chemistry Reviews **249**, 31 (2005); G. van der Laan and I.W. Kirkman, Journal of Physics: Condensed Matter **4**, 4189 (1992).
16. M.W. Haverkort, Z. Hu, A. Tanaka, W. Reichelt, S.V. Streltsov, M.A. Korotin, V.I. Anisimov, H.H. Hsieh, H.J. Lin, C.T. Chen, D.I. Khomskii, and L.H. Tjeng, Physical Review Letters **95**, 196404 (2005).
17. G.P. Zhang, G.T. Woods, E.L. Shirley, T.A. Callcott, L. Lin, G.S. Chang, B.C. Sales, D. Mandrus, and J. He, Phys Rev B **65**, 165107 (2002).
18. M. Abbate, H. Pen, M.T. Czyzyk, F.M.F. de Groot, J.C. Fuggle, Y.J. Ma, C.T. Chen, F. Sette, A. Fujimori, Y. Ueda, and K. Kosuge, Journal of Electron Spectroscopy and Related Phenomena **62**, 185 (1993); A. Gloter, V. Serin, C. Turquat, C. Cesari, C. Leroux, and G. Nihoul, European Physical Journal B **22**, 179 (2001).
19. C. Ma, H.X. Yang, Z.A. Li, Y. Ueda, and J.Q. Li, Solid State Communications **146**, 30 (2008).
20. R. Enjalbert and J. Galy, Acta Crystallographica, C **C42**, 1467 (1986).
21. E. Goering, O. Muller, M. Klemm, M.L. denBoer, and S. Horn, Philosophical Magazine B **75**, 229 (1997).
22. V. Eyert and K.H. Hock, Physical Review B (Condensed Matter) **57**, 12727 (1998).
23. G.T. Woods, G.P. Zhang, T.A. Callcott, L. Lin, G.S. Chang, B. Sales, D. Mandrus, and J. He, Phys Rev B **65**, 165108 (2002).
24. H. Smolinski, C. Gros, W. Weber, U. Peuchert, G. Roth, M. Weiden, and C. Geibel, Physical Review Letters **80**, 5164 (1998).
25. J. Nordgren, G. Bray, S. Cramm, R. Nyholm, J.E. Rubensson, and N. Wassdahl, Review of Scientific Instruments **60**, 1690 (1989).
26. K.E. Smith, C. McGuinness, J.E. Downes, P.J. Ryan, S.L. Hulbert, J.M. Honig, and R.G. Egdell, Mater. Res. Soc. Symp. Proc. **755**, DD1.1.1 (2003).
27. A.R.H. Preston, B.J. Ruck, L.F.J. Piper, A. DeMasi, K.E. Smith, A. Schleife, F. Fuchs, F. Bechstedt, J. Chai, and S.M. Durbin, Phys Rev B **78**, 155114 (2008).
28. T. Schmitt, L.C. Duda, M. Matsubara, A. Augustsson, F. Trif, J.H. Guo, L. Gridneva, T. Uozumi, A. Kotani, and J. Nordgren, Journal of Alloys and Compounds **362**, 143 (2004).
29. K.E. Smith, Solid State Sciences **4**, 359 (2002).
30. G.P. Zhang, T.A. Callcott, G.T. Woods, L. Lini, B. Sales, D. Mandrus, and J. He, Physical Review Letters **88**, 077401 (2002).
31. L.C. Duda, T. Schmitt, J. Nordgren, P. Kuiper, G. Dhalenne, and A. Revcolevschi, Physical Review Letters **93**, 169701 (2004).
32. M. van Veenendaal and A.J. Fedro, Physical Review Letters **92**, 219701 (2004); G.P. Zhang and T.A. Callcott, Physical Review B (Condensed Matter and Materials Physics) **73**, 125102 (2006); G.P. Zhang, T.A. Callcott, G.T. Woods, L. Lin, B. Sales, D. Mandrus, and J. He, Physical Review Letters **92**, 219702 (2004); Y. Zhang, S. Wang, T. Learmonth, L. Plucinski, A.Y. Matsuura, S. Bernardis, C. O'Donnell, J.E. Downes, and K.E. Smith, Chemical Physics Letters **413**, 95 (2005).

33. E. Stavitski and F.M.F. de Groot, Micron **41**, 687 (2010).

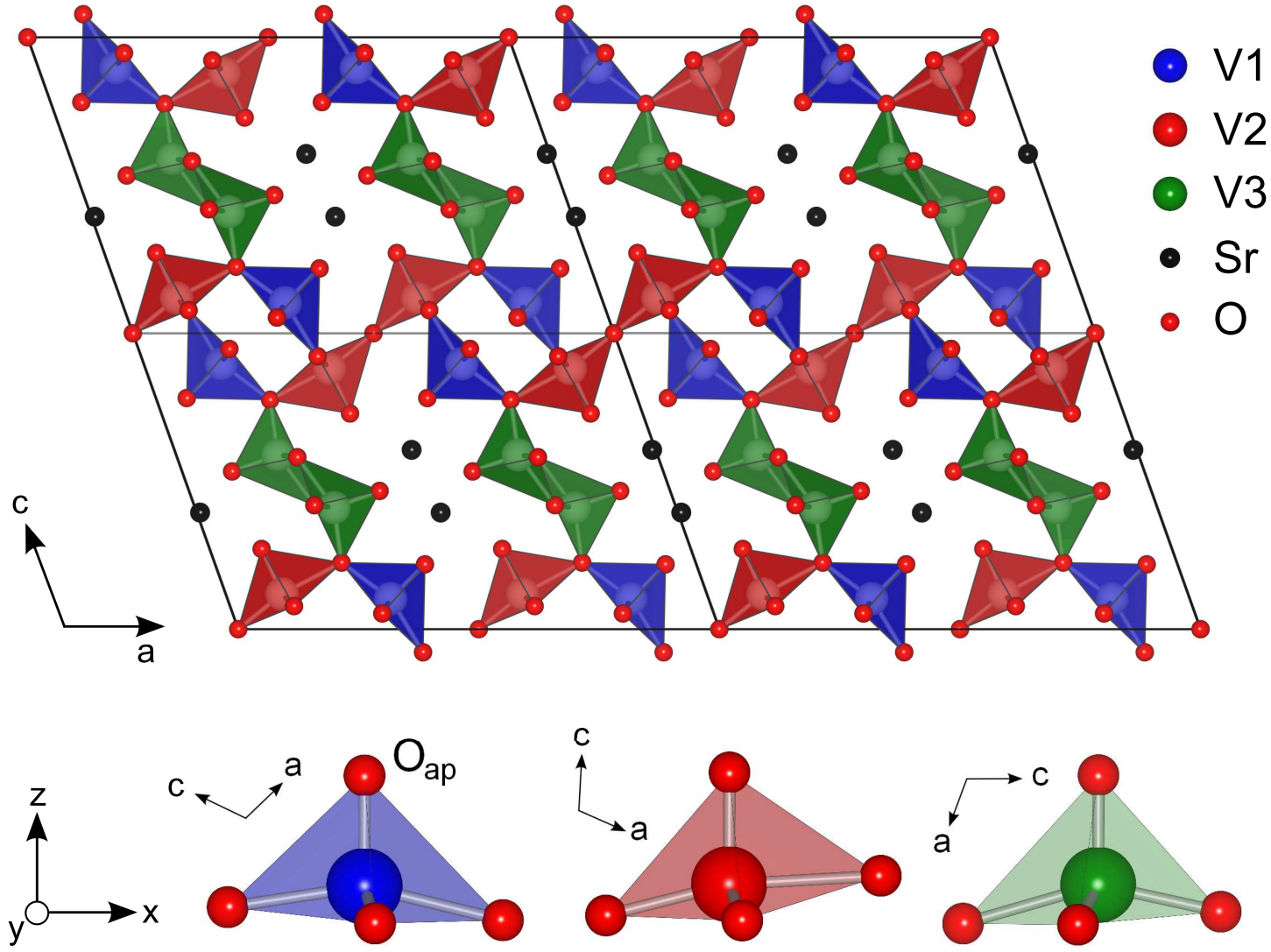

Figure 1 BA11649 14SEP2011

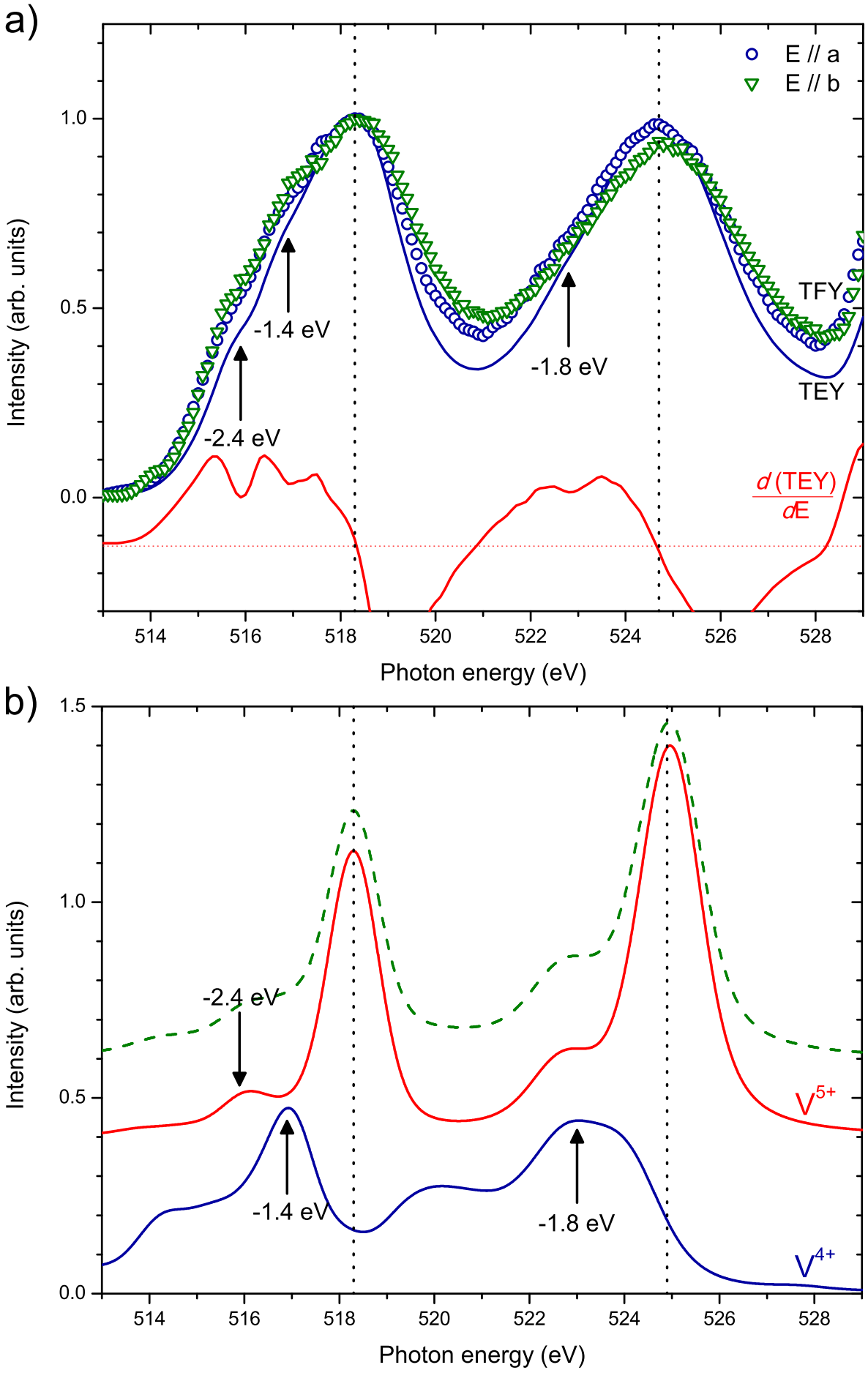

Figure 2 BA11649 14SEP2011

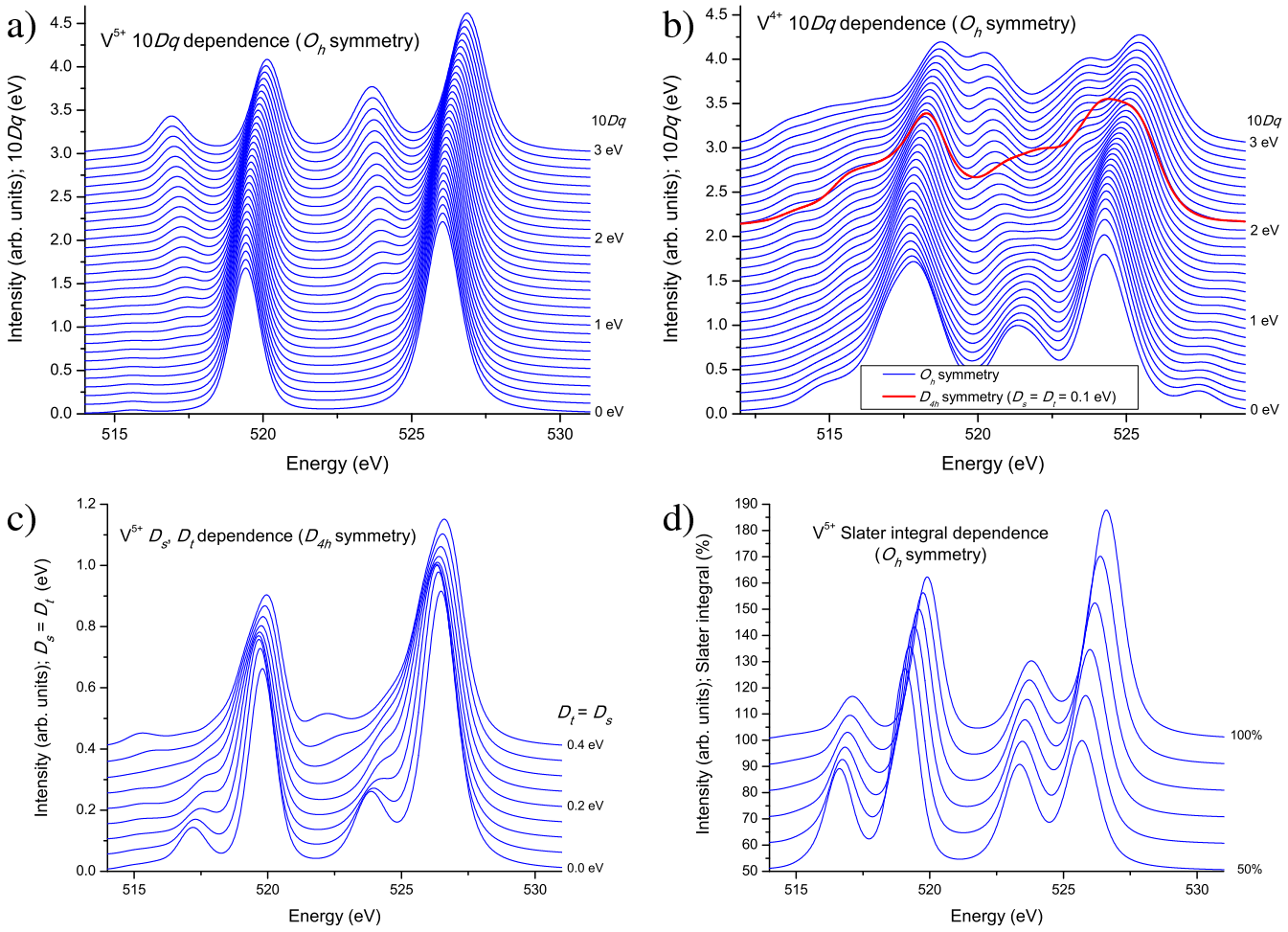

Figure 3 BA11649 14SEP2011

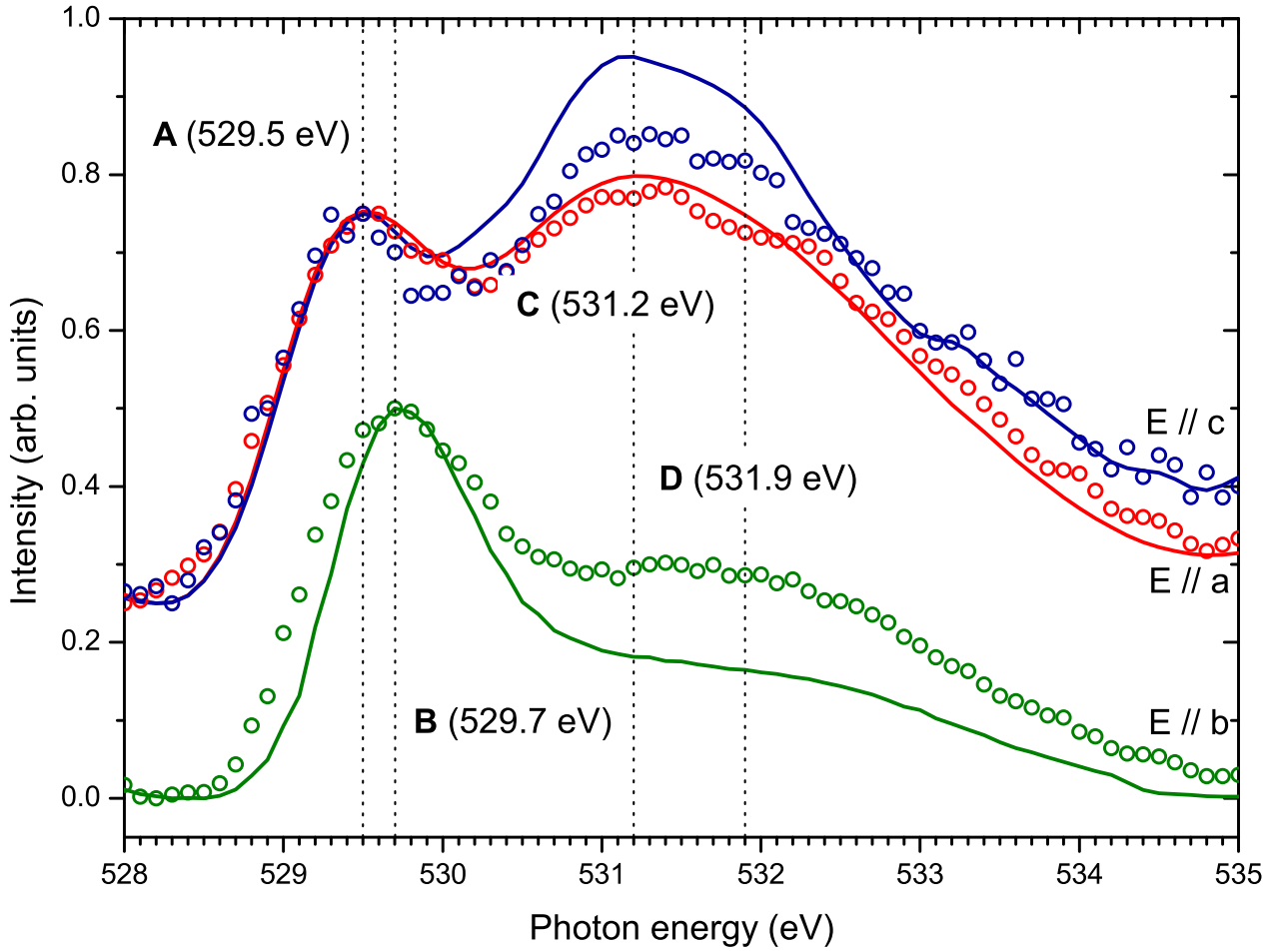

Figure 4 BA11649 14SEP2011

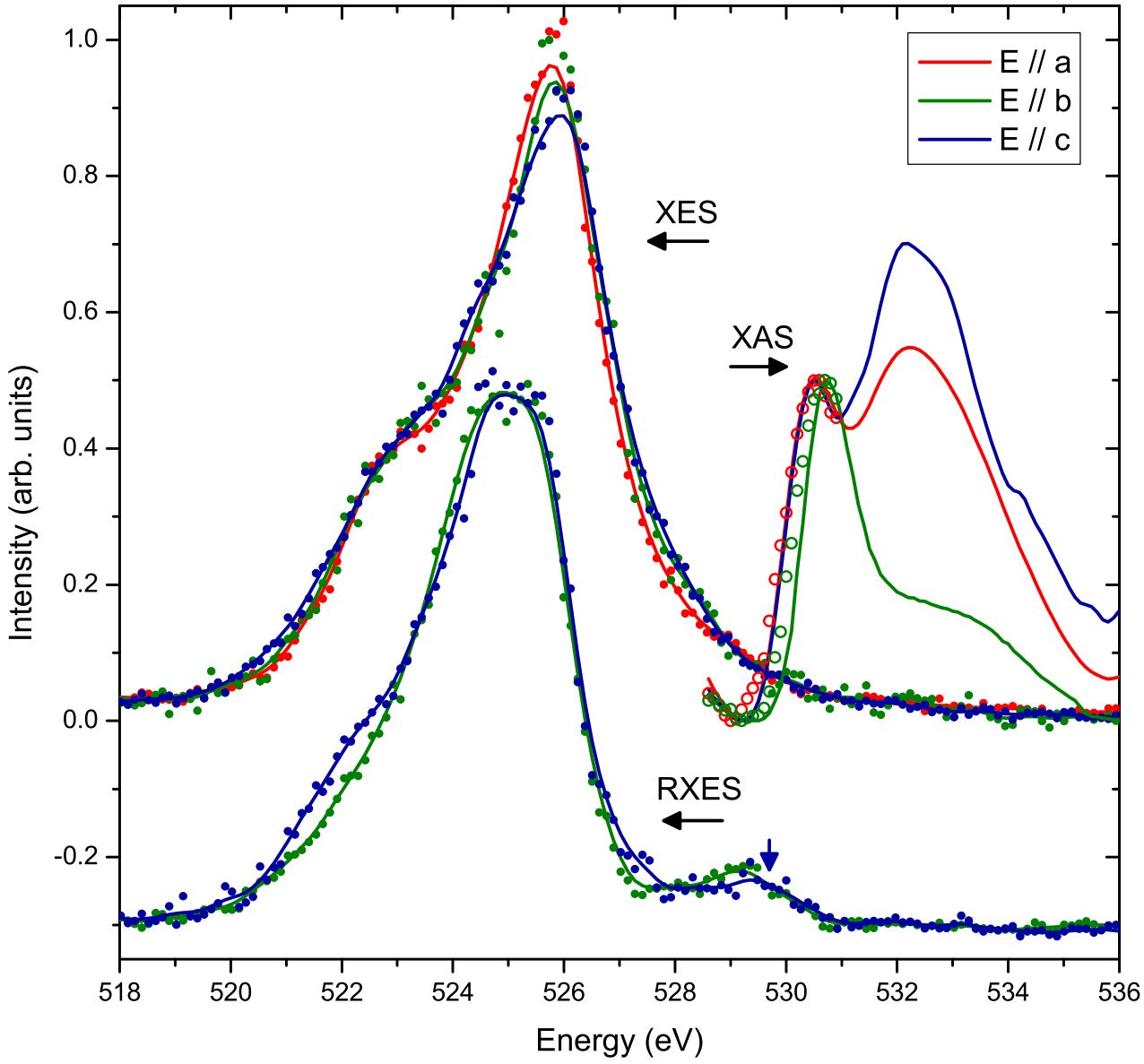

Figure 5 BA11649 14SEP2011

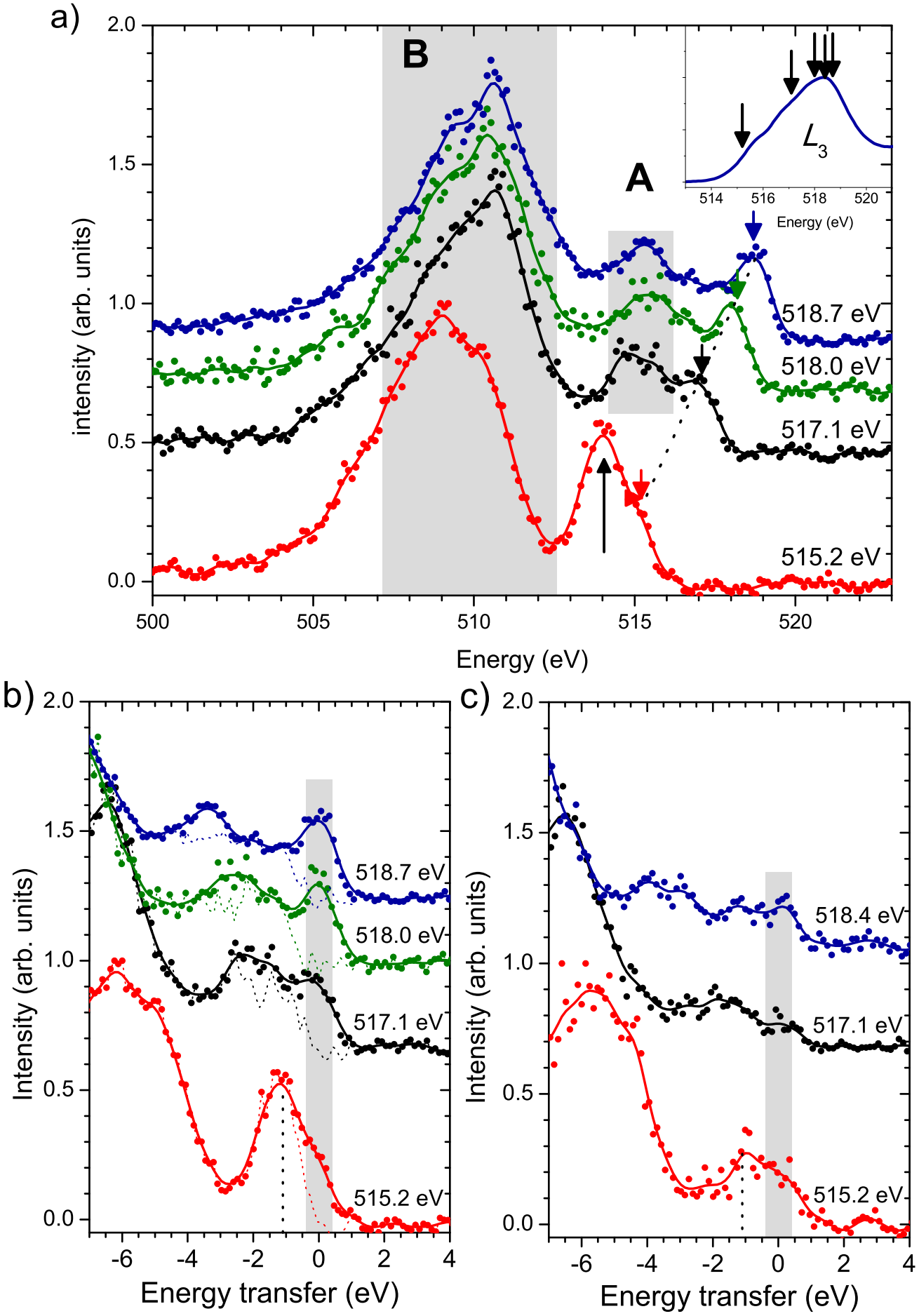

Figure 6 BA11649 14SEP2011

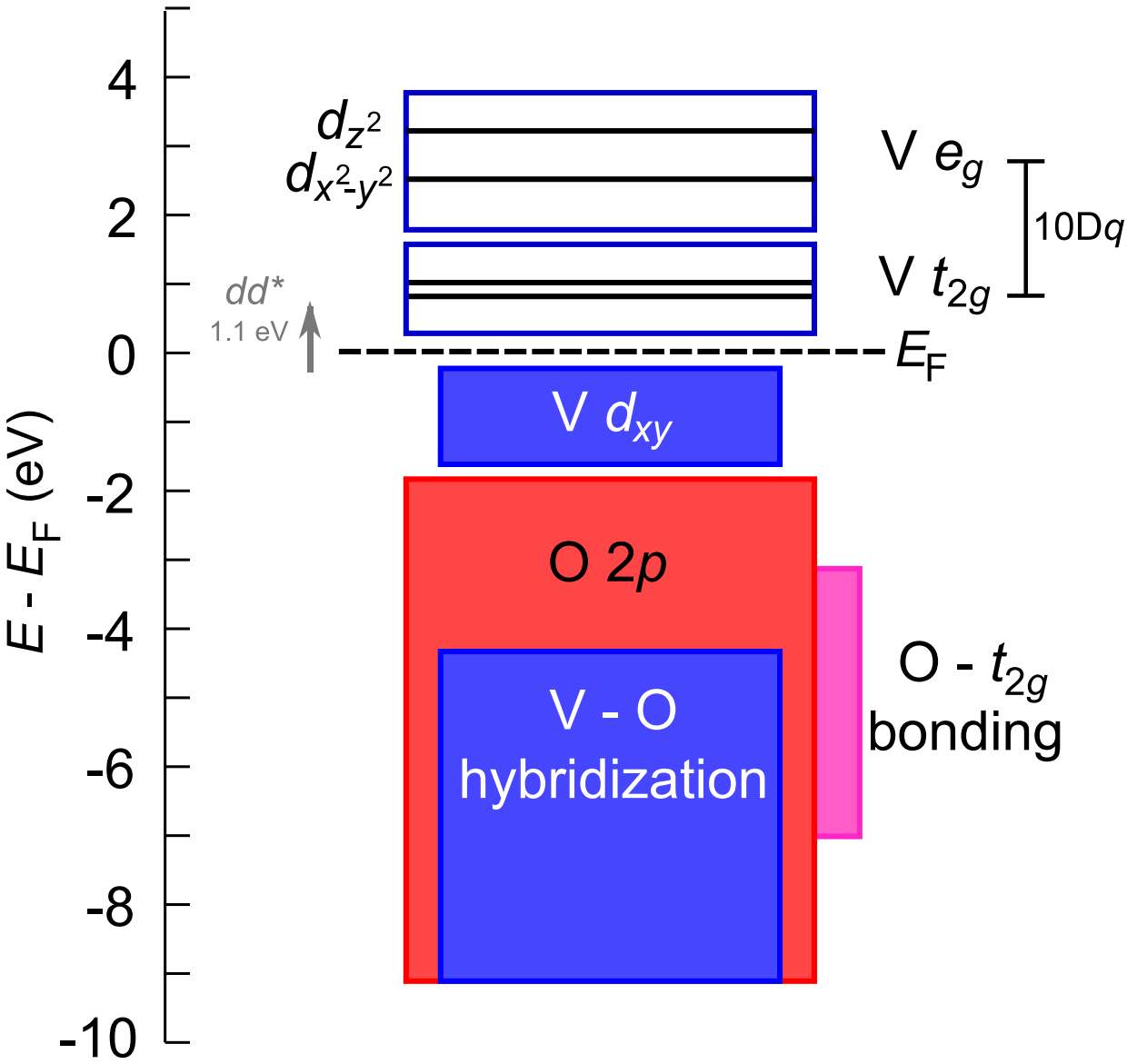

Figure 7 BA11649 14SEP2011